Electrocoalescence of Water Droplets in Sunflower Oil Using a Novel Electrode Geometry

Bin Li[a,b], Vincenzino Vivacqua[b],Junfeng Wang[a], Zhentao Wang[a], Zhiqian Sun[c], Zhenbo Wang[c], Mojtaba Ghadiri[b, *]

[a] School of Energy and Power Engineering, Jiangsu University, Zhenjiang 212013, China

[b] School of Chemical and Process Engineering, University of Leeds, Leeds LS2 9JT, UK

[c] State Key Laboratory of Heavy Oil, China University of Petroleum (East China), Qingdao 266580, China

Abstract: Electrocoalescence is an energy-efficient and environmentally-friendly process for breaking water-in-oil emulsions. It has been used extensively in the oil and petroleum industries. However, the current technology requires long residence times, giving rise to bulky vessels for industrial scale operations and making it less attractive for offshore application. It is also highly desirable to develop compact devices for down-the-well use. In this study, the performance of a novel electrode geometry, a ladder-shaped set of electrodes through which the emulsion flows, is assessed for enhancing the electrocoalescence, hence providing the potential for a compact design. The electrodes are formed into a V shape, with the apex pointing towards the direction of flow. This configuration enables nesting a series of electrodes in a compact form. Furthermore, the water-in-oil emulsion flows through the electrodes rather than passing by them, thus maximizing the effect of the electric field for coalescence. The system

---
* Corresponding author. Tel: +44 113 343 2406; Fax: +44 113 343 2384.
  E-mail address: M.Ghadiri@leeds.ac.uk (M. Ghadiri).

under study uses dispersed water droplets in sunflower oil, flowing in a narrow rectangular duct through the electrodes, providing essentially a two-dimensional flowing stream. The performance of this design is investigated for different electrical parameters (i.e. electric field intensity, frequency and waveform), fluid physical properties (i.e. conductivity and water content) and residence time. Of the three types of electric field waveform (i.e. half-sinusoidal, square and sawtooth), sawtooth performs best at high conductivities. Experiments reveal the existence of optimal values of electric field intensity, electric field frequency, salt concentration and water concentration, where the coalescence efficiency is maximum for the current design. Numerical simulation of the electrocoalescence process is conducted to assess the influence of various geometric and process parameters on the coalescence mechanisms of the V-shape electrodes. The outcome of this work is potentially useful for optimizing the design of compact and efficient oil-water separators.

Keywords: Electrocoalescence; Electrode design; Pulsatile direct current; Phase separation; Oil treatment

1. Introduction

Crude oil, extracted from the reservoirs, contains a significant amount of saline water in dispersed phase accompanied by resins, asphaltenes, and paraffins, which stabilize the dispersion as they act as surfactant [1]. The amount of water also increases with the age of the well [2]. Moreover, some oil production methods, e.g. steam-assisted gravity

drainage (SAGD), generate a large amount of water, which has reached as much as 90 wt% in recent years [3]. As a consequence, stable water-in-oil (W/O) emulsions are readily formed during crude oil production stage, causing detrimental problems in the oil industry, such as equipment corrosion, catalyst poisoning and extra transportation cost [2, 4]. Therefore, efficient methods to remove the water phase from the oil phase are highly desirable and will have significant financial benefits. Several techniques [5-9] have been applied to improve the separation efficiency. Electrostatic demulsification stands out among these methods because of its low operating costs and environmentally-friendly nature [2]. However, the cost of conventional electrocoalescers is high as the vessels are very large to provide long residence times (typically 30-40 minutes [10]) necessary for phase separation. Hence, novel electrocoalescers with better performance and a shorter residence time, thus more compact, would be highly desirable, particularly enabling dewatering application down the well. This is addressed in this work by evaluating a novel electrode design, based on the concept proposed by Vivacqua et al. [11], and using several electric field waveforms.

With respect to electric field patterns, alternating current (AC), direct current (DC), pulsatile DC and their combinations have been utilised to enhance electrocoalescence. Taylor [4] reviewed the mechanisms of phase separation for different electric fields. Bailes et al. [12, 13] investigated the mechanism of pulsed DC fields with insulated electrodes. They showed that coalescence was mainly through induction of dipoles on the droplets, and that the use of pulsatile fields resulted in enhanced coalescence.

Recently, Vivacqua et al. [14] conducted experiments with a pair of ladder-shape bare electrodes in pulsed DC fields and found that the dominant coalescence mechanism between droplets was dipole-dipole interaction at low electric field intensity, whereas electrophoresis became predominant at higher intensities. Furthermore, their work showed that the pulsed electric fields with optimal field parameters (intensity, frequency, and waveform) had a better dehydration performance than that of constant DC electric fields. Notwithstanding a number of research works [14-19] conducted on the effect of the electric waveform on electrocoalescence, the understanding of the influence of the waveforms is still limited, with some contrasting conclusions. Lundgaard et al. [16] and Lesaint et al. [17] ranked the efficiency of AC waveforms as square > sinusoidal > triangular, which is similar to the results obtained by Li et al. [20]; whereas Mousavi et al. [15] reported that the coalescence efficiency of pulsed DC triangular and half-sinusoidal waves was superior to that obtained with square waves. Flat electrodes were used in the work of Lundgaard et al. [16] and Mousavi et al. [15], while cylindrical electrodes were used in the work of Lesaint et al. [17]. In another study, Ingebrigtsen et al. [19] reported similar coalescence efficiency for half-sinusoidal and square waves.

Regarding electric field parameters, namely electric field intensity, frequency and waveform, a number of studies have addressed this topic. Williams et al. [21] reported that the coalescence efficiency improved with increasing electric field intensity. However, droplets break up if the intensity is set to a too high value, resulting in the formation of fine secondary droplets that are much more difficult to remove from the oil [11, 22-28]. One of the pioneering investigations on the effect of electric field

frequency on droplets coalescence was conducted by Brown and Hanson [29]. By applying oscillating fields, they identified an optimum frequency and a minimum critical electric field intensity for coalescence. Vivacqua et al. [14] addressed the influence of field frequency as a function of the field intensity. At low values of the field intensity, typically around 67 to 134 kV m^{-1}, an optimum frequency was obtained at which the average droplet enlargement was most significant. However, the role played by frequency was found to be less important at higher electric fields. Mousavi et al. [15] conducted experiments on drop-drop and drop-interface coalescence under pulsatile electric fields, and determined a threshold frequency above which partial coalescence pattern switched to complete coalescence pattern. Particularly, for drop-drop coalescence, the threshold frequency depended on the pulsatile field amplitude and initial droplet size. Li et al. [3] carried out investigations on the electro-dehydration of crude oil emulsions, and found that the frequency of the applied voltage had a notable influence on the dehydration efficiency.

The emulsion physical properties have a significant influence on the droplets behaviour [30-34]. He et al. [35] reported that the droplet deformation time (i.e. the time required for the droplet to reach its final shape) is sensitive to interfacial tension and oil viscosity. The water phase in crude oil contains dissolved salts, which influence water conductivity significantly. Vivacqua et al. [36] developed a Level-Set approach to model the electrocoalescence and found numerically that as the conductivity was increased, partial coalescence produced larger secondary droplets and the largest was at 10^{-3} S m^{-1}. Moreover, Hamlin et al. [37] reported the existence of a critical

conductivity, below which the droplets partially coalesced, while above which the droplets bounced off each another. Zhang et al. [38] investigated the influence of salt concentration on the electro-dehydration process and reported that the addition of sodium chloride in the aqueous phase could dramatically increase the emulsion dehydration efficiency.

With respect to the type of electrodes used, insufficient attention has been devoted to the geometry of the electrodes, which are usually flat plates, grids, or coaxial cylinders, where the emulsion essentially flows over and parallel to the electrode surface [1, 11]. Eow and Ghadiri [39] used five different two-dimensional electrode designs to study the effect of electric field on drop-drop coalescence. They reported that drop-drop coalescence readily occurs when the electric field is applied in the same direction as the line joining the centres of the two drops. The grounded plate electrode, when made hydrophilic, is able to retain a layer of water on its surface and that enhances drop-interface coalescence, further assisting the separation of the dispersed drops from a flowing continuous oil phase. Xu and Li et al. [40] proposed three types of electrode geometry (folded plate electrodes, mesh electrodes and grid electrodes), and found that the electric field created by the proposed electrodes could aid the dehydration process by optimizing the electric field distribution and the droplet migration. Furthermore, the results indicated that the non-uniform fields formed by the proposed electrodes could accelerate the movement of water drops, facilitating coalescence. Furthermore, most of the electrodes used in commercial electrocoalescers are usually insulated to avoid short-circuiting. However, coalescers with bare electrodes have a higher efficiency, because

water droplets become charged by direct contact with the electrodes and thereby have rapid electrophoretic motion [14]. In the light of the above considerations, it appears that the optimal design of efficient industrial electrocoalescers is far from being identified. The overall picture related to the influence of electrode geometry and its insulation and type of electric field waveform is fragmentary and sometimes contradictory. The presence of bare electrodes ensures a higher rate of collision between drops due to electrophoresis and dramatically increases the coalescence rate, but it is prone to short-circuiting. The electrode geometry determines the electrostatic interactions [39] between drops and also affects the flow field. In the work reported here, the performance of a novel bare electrode setup with the shape of a ladder assembled in V shape is tested. The effects of the field intensity, frequency, and waveform, salt content, and residence time on the separation efficiency are assessed. The outcome of this work is potentially useful for optimizing the design of oil-water separation devices.

2. Experimental set-up and procedures

Deionised water (the dispersed phase) and sunflower oil (the continuous phase, from Morrisons, Ltd) were used to form a water-in-oil (W/O) emulsion, using a mechanical stirrer (IKA Werker), having a maximum speed of 2000 rpm. In the experiments here the stirrer speed was set at 500 rpm for 1 hour for preparing the emulsion. The properties of the experimental liquids are reported in Table 1a. The procedure by which the liquids properties were measured is described by Mousavichoubeh et al. [22]. The interfacial

tension between the deionised water and sunflower oil was 25 mN m^{-1} with no surfactant being introduced into the emulsions. The conductivity of the deionised water changed negligibly during the experiments, except those for which the effect of conductivity was investigated. The variation of the permittivity was neglected, considering that the dielectric constant of water is much higher than that of the oil.

A schematic diagram of the experimental set-up is shown in Fig. 1a.   A drawing and a picture of the electrode geometry are given in Fig. 1b. The electrodes are inserted into a narrow rectangular duct, which is made of Perspex, providing essentially a two-dimensional flow to facilitate observation by video recording. The electrodes are bare and made of brass. The use of this type of V shape for the electrodes increases the contact area between the droplets and electrodes. With bare electrodes, droplets get charged when intercepted by the electrodes. The coalescence is thus promoted both by dipole-dipole interactions and electrophoresis [14]. The coalescer is installed vertically with the emulsion flowing downward. Each half electrode has eight bars with a uniform separation of 3 mm between them. The length of the bar is 10 mm, and the width is 1 mm, as shown in Fig. 1b. The distance between the high voltage and grounded electrodes is 10 mm. A 50° inclination angle is selected to promote rolling of the water droplets over the electrode surface towards the central region.

A micropump (Watson-Marlow, 5003U), capable of delivering flow rates in the range 0.1-3.0 L min^{-1}, is used to pump the emulsion to the electrocoalescer. The high voltage electrode is connected to a waveform generator, feeding a Trek 20/20C high voltage amplifier. The bottom electrode is grounded. Hence an electric field is set up

between the pair of electrodes. The emulsion then flows through a narrow 5 mm thin view port, made of glass, to facilitate observation of the droplets growth by means of a high-speed digital video camera (Photron FASTCAM SA5), equipped with a micro-lens (NAVITAR 12 × Zoom Lens). Video recording is made at 30 frames per second (fps). A halogen lamp (Dedolight DLHM4-300) is used for lighting. The droplet size distribution is measured by ImageJ software (https://imagej.net) with an in-house code developed to identify the overlapping ones and separate them to measure their size. The flow rate of the emulsion is 50 mL min^{-1} (corresponding to a Reynolds number of 0.005 based on the hydraulic diameter of the duct) in most of the experiments, varying only when the effect of the residence time is investigated, so creeping flow regime prevails. The initial droplet size is around 0.16 mm, so the shear rate exerted on the droplets is negligible. The water content of the emulsion is 2 vol% in all the experiments, except when the effect of the water content is addressed. The focus of this work is on gaining a better understanding of how to enhance the coalescence and develop a compact design of electrodes which can increase the coalescence rate and efficiency and reduce the vessel volume. The model emulsions used in the experiment are prepared with water and sunflower oil and no surface active agent is added. This makes the preparation of stable emulsions with fine droplets and high water content difficult. So emulsions with low water content and large droplet size are used in the first instance to provide a controlled model system to understand the fundamentals of the process. Obviously, for commercial applications, crude oil will have to be tried. However, the properties of the water-in-sunflower oil emulsion are suitable to demonstrate the concept. The

experiments were performed at 20±2 °C. New oil is used each time to conduct the experiments under different working conditions. Each experiment was repeated three times, and the error bars in this paper are calculated as standard errors.

<Fig.1 Experimental rig and electrode design>

3. Results

The droplet images, captured by the high-speed camera from the view port are shown in Figs. 2 (a) and (b), before and in the presence of the electric field, respectively. In Fig. 2 (c) the droplet diameter distributions (by number) before and after the application of electric field are reported. The arithmetic mean diameter before the application of the electric field is around 160 μm. The emulsion was stable for a duration longer than 30 min, i.e. much longer than the experiment time, as indicated by no notable change in the size distribution at 30 min rest time (not shown for brevity). From Fig. 2, a remarkable droplet enlargement is observed using the present electrode design.

<Fig.2 Representative snapshots of emulsion from the view port and initial droplet size distribution. (a): in the absence of electric field; (b): after the application of the electric field; (c): droplet size distribution (by number) before and after the application of electric field. The experimental conditions are: sunflower oil with 2 vol% deionised water; constant waveform; electric field intensity (E) of 200 V mm^{-1}.>

In the current design, the interaction between the water droplets and bare electrodes plays a significant role in the electrocoalescence mechanism. The electric field is nonuniform near both electrodes and water droplets, as shown in Fig. 3a. Therefore, the average electric field intensity ($E = \frac{\text{Eletric voltage}}{\text{Electrode distance}}$) is reported. The droplets behaviour between the V-Shape electrodes is shown in Fig. 3b. In the presence of an electric field, a significant enlargement of the water droplets is observed. They get charged when contacting the electrodes directly, as a result of which an electrostatic force is set up due to charge transfer, moving them to the opposite electrode (yellow outline in Fig. 3b (i), (j), (k), and (l)). The droplets stream through the electrodes, having their motion parallel to the electric field. This enhances their coalescence significantly, both in the bulk (purple outline in Fig. 3b (b), (c) and (g), (h)) and also on the electrode surface, forming a water film. Large droplets may also adhere to the electrodes, as shown in the orange outline in Fig. 3b (c) and (d), where the fine droplets have coalesced on the film or the former. The wettability of the electrode, therefore, influences the coalescence pattern. Moreover, when the droplets are intercepted by the bare electrodes, their forward motion is retarded, followed by rapid coalescence with the water film on the electrodes. In the present work, drop-interface partial electrocoalescence (red outline in Fig. 3b (f), (g), (h)) and drop-drop non-coalescence (blue outline in Fig. 3b (e), (f)) are observed, which have adverse effects on the coalescence efficiency [1]. Video records showing the process are provided in the supplementary data file.

In order to accomplish a quantitative assessment of the electrical and physical parameters influencing the performance of the electrodes, a definition of the coalescence efficiency is needed. In the work of Vivacqua et al. [14], the size ratio $\frac{d_{out}}{d_{in}}$ was utilised to calculate the efficiency. This is not practical in our case because of too large droplet number. Considering that all the droplets larger than 500 μm are separated very rapidly from oil phase in a downstream settler, the coalescence efficiency is defined by in Eq. (1). Droplets smaller than 500 μm would obviously coalesce too, but they would be too small to be separated easily, so Eq. (1) would be a conservative way of estimating coalescence efficiency.

$$\text{Coalescence efficiency} = \frac{\text{Volume of droplets larger than 500 μm}}{\text{Total view port volume} \times \text{initial water content}} \quad (1)$$

An equivalent spherical droplet volume is used to calculate the efficiency, as most of the droplets are spherical, except few very large ones which can deform easily in the electric field. In our calculation of efficiency, all the droplets are analysed once, because of the low frame acquisition rate (30 fps) and sufficiently long time intervals (about 2 s) between two consecutive frames analysed. This ensures that completely different droplet populations are considered in each frame.

The performance of the new design (V shape) may be compared with that of the flat design [14, 39] in terms of coalescence efficiency using sunflower oil emulsion

12

with 2 vol% water. Constant DC wave is applied and the average electric field intensity is 200 V mm^{-1}. For a residence time of 8.5 s for both cases, the coalescence efficiency is about 27 % for the V shape electrode and 18 % for the flat electrode.

3.1   Electric field intensity

The coalescence efficiency of the W/O emulsion subjected to different pulsatile electric field intensities (peak values reported here) and waveforms is reported in Fig. 4a. In all cases, the frequency is kept at 100 Hz. As a first remark, the efficiency increases with the field intensity before reaching a maximum value; then it decreases at higher intensities for all the four waveforms. Therefore there exists an optimum field intensity. The dipole-dipole coalescence mechanism plays a dominant role at low intensities (< 200 V mm^{-1} for DC constant, 300 V mm^{-1} for square and half-sinusoidal and 400 V mm^{-1} for sawtooth waveforms) [14]. Coalescence by electrophoresis mechanism becomes more and more significant with increasing field intensity [14]. At the optimum field intensity, the combination of the two mechanisms of dipole-dipole coalescence and electrophoresis provides the best coalescence efficiency. At field intensities higher than the above values, short-circuiting occurs, which leads to a decrease in efficiency. This is shown in Fig. 4b, where the electric field intensities at 300 and 500 V mm^{-1} are compared. At 300 V mm^{-1} (Fig. 4b (i)), the electric field follows the prescribed pattern. However, at 500 V mm^{-1} (Fig. 4b (ii)), the actual intensities applied to the emulsions decrease significantly, and become actually lower than that of 300 V mm^{-1}, resulting from the occurrence of short-circuiting. So at high intensities, the decrease in efficiency

is due to a lower average field intensity caused by short-circuiting as well as the occurrence of droplet break-up and partial coalescence which produces tiny secondary droplets [3, 14, 15, 23, 40, 41].

< Fig. 4: (a) Coalescence efficiency with half-sinusoidal, square and sawtooth DC fields at varying electric field intensity. The electric field frequency applied is the optimum frequency of 100 Hz for all the three pulsatile waveforms. Comparison with constant DC fields. (b) Snapshots of experimental electric intensities applied to the emulsions: (i) Square waveform, 5 Hz, 300 V mm^{-1}; (ii) Square waveform, 5 Hz, 500 V mm^{-1}.>

Interestingly, different waveforms correspond to different optimum intensities, i.e. 200 V mm^{-1} for constant, 300 V mm^{-1} for half-sinusoidal and square, and 400 V mm^{-1} for sawtooth waveforms. Lesaint et al. [17] reported that the root mean square (RMS) of the electric field can represent the effectiveness of different electric field waveforms. The theoretical RMS values of the electric field of the four waveforms used here are shown in Table 1b. At a given peak field intensity, higher RMS values are associated with the square and half-sinusoidal waveforms, compared to sawtooth waveform. However, with the data scatter present, it cannot conclusively be shown which waveform performs best at all intensities. The source of the scatter may come from the initial emulsion, where a few large droplets may exist and they may coalescence with small ones. Also the droplet size distribution may vary slightly from experiment to experiment that may contribute to additional error. Furthermore, the electrodes cannot

always hold up large droplets to form water films, which influence drop-interface coalescence significantly. The constant field has a larger RMS value than those of the pulsatile electric fields. However, its efficiency is lower than the other waveforms for field intensities larger than 200 V mm^{-1}. This demonstrates that the pulsatile nature of the field by itself plays a significant role in promoting coalescence. It is noteworthy that, at low field intensities (E < 250 V mm^{-1}), the efficiency of constant field is actually higher compared to pulsatile fields, whereas at high field intensities (E > 320 V mm^{-1}), pulsatile fields perform much better. The role played by the electric field frequency needs further studies as only 100 Hz was used here.

3.2 Electric field frequency

The effect of varying the electric field frequency of various waveforms on the coalescence efficiency is shown in Fig. 5. The field intensities used in this case are the optimum values for all the three pulsatile waveforms, i.e. half-sinusoidal and square waves of 300 V mm^{-1}, and sawtooth wave of 400 V mm^{-1}, as at the optimum intensity, the effect of waveform pattern is reduced, which helps to focus on investigating the effect of frequency. The efficiency shows a maximum value at an intermediate frequency of 100 Hz for all the waveforms. The dependence of the efficiency on frequency could be interpreted considering that the oscillation of droplets and collision rate of neighbouring droplets are enhanced with increasing frequencies, in so far as the droplets can mechanically respond to the electric field, thus enhancing the coalescence. At the optimum frequency (f =100 Hz), the droplets oscillation and deformation extent

are maximal as recently analysed by Li et al. [20]. At higher frequencies (f >100 Hz), both the deformation extent and oscillation amplitude of droplets decrease significantly with increasing frequencies, accounting for a reduction in the coalescence efficiency. The efficiency of the constant field at the optimum intensity (200 V mm^{-1}) is given in dotted line for comparison in Fig. 5. For frequencies in the range of 60-200 Hz, the pulsatile electric fields perform better than the constant field, and a remarkable improvement is observed at the optimal frequency (100 Hz). Comparing the performance of different field waveforms at varying field intensities (Fig. 4a) and frequencies (Fig. 5), the rank order varies with frequency. However, for 100 Hz, it is in the order square > half-sinusoidal > sawtooth waveforms. For this case the trend is in agreement with that reported by Lundgaard et al. [16] and Lesaint et al. [17].

<Fig. 5 Coalescence efficiency with half-sinusoidal, square and sawtooth DC fields at varying electric field frequency. The applied electric field intensities are the optimum values: half-sinusoidal and square wave of 300 V mm^{-1}, sawtooth wave of 400 V mm^{-1}. Comparison with constant DC fields of 200 V mm^{-1}.>

3.3   Salt concentration

Sodium chloride (NaCl) was added to water to vary the conductivity. The values of conductivity obtained are shown in Table 1c. E=200 V mm^{-1} and f=100 Hz are applied. The average applied field intensity is 200 V mm^{-1} for all the cases here to avoid short-circuiting, which occurs more easily at high salt concentration and high water content.

The variation of the coalescence efficiency with salt concentration in pulsatile fields is reported in Fig. 6a. At low concentrations, with increasing salt content, higher charges are transferred to the droplets upon contact with the bare electrodes. Larger electrostatic forces are induced and the dipole-dipole coalescence is thereby enhanced remarkably. Moreover, the electrophoresis coalescence mechanism is enhanced significantly, as droplets accelerate more rapidly with increasing conductivity. The optimal NaCl concentration is 2 g L^{-1}, after which the efficiency declines for the half-sinusoidal and square waveforms, but not for the sawtooth waveform. Droplet disintegrations and occasional short-circuiting account for the decrease of efficiency at high concentrations. As the conductivity is increased, the dipole moment induced onto the droplet increases [14]. This brings about a larger deformation of the droplet, which tends to also increase the disintegration of droplets. With increasing salt concentration, the charge movement becomes faster, but also the electrostatic force becomes larger as more ions are in the emulsion. Therefore, the disintegration of droplets is enhanced. Another noteworthy point is that, the coalescence efficiency with sawtooth waveform shows no change at 3 g L^{-1}, while with square and half-sinusoidal waves it decreases significantly. This might have resulted from the lower RMS value of sawtooth compared to those of the other two waveforms. Generally speaking, increasing the salt content, short-circuiting and droplet disintegration will occur more easily. However, lower RMS value means lower electric field intensity. Therefore, the probability of short-circuiting and disintegration in low RMS electric field is reduced.

3.4 Water concentration

The effect of water content on the coalescence efficiency is shown in Fig. 6b. With respect to half-sinusoidal and square waveforms, the efficiencies increase first, with their maximum around 3 vol% water content and then show no notable further variation with increasing water concentration to 4 vol%. However, the sawtooth waveform has a consistent increase from 1 to 4 vol%. Higher water contents mean shorter inter-droplet distances. The dipole-dipole coalescence mechanism is thus enhanced with increasing water content due to its short-range nature [14]. Moreover, the electrophoresis coalescence mechanism is also enhanced, because of the increasing likelihood of a droplet to contact other droplets with increasing water concentration. Furthermore, larger concentration means more droplets go through the electrodes, leading to more charge transferred to the coalescence region. As a result, the electrophoresis coalescence is enhanced. The results are in agreement with Harpur et al.'s research [42] and the previous experimental work of Vivacqua et al. [14] using a pair of ladder-shape electrodes designed by Eow and Ghadiri [39]. They reported that the coalescence efficiency of contiguous droplets is higher than that of droplets with wider inter-droplet distances. By further increasing the water content to 4 vol%, larger droplets are formed. When the capillary number (given in Eq. (2)) of the enlarged droplets exceeds a critical value, the droplets break into tiny droplets, reducing the separation efficiency of the system [14, 22, 23].

$$Ca_{el} = \frac{E_0^2 D \varepsilon_{oil}}{\gamma} \tag{2}$$

where E_0 is the peak value of the applied field intensity, D is the droplet size, ε_{oil} is the

oil permittivity and γ is the oil/water surface tension. In addition, short-circuiting occurs easily at high water concentration.

<Fig. 6: (a) Coalescence efficiency with half-sinusoidal, square and sawtooth DC fields at varying NaCl concentration. (b) Coalescence efficiency with half-sinusoidal, square and sawtooth DC fields at varying water concentration. (c) Coalescence efficiency with half-sinusoidal, square and sawtooth DC fields at varying residence time. The electric field intensities and frequencies applied are 200 V mm^{-1} and 100 Hz, respectively, for all the three waveforms.>

3.5   Residence time

Residence time is an important variable as it determines the volume of the vessel. The emulsion flow rates used are 50, 100, and 150 mL min^{-1}, which correspond to residence time of 6, 3, and 2 s, respectively. The Reynolds numbers of duct for the corresponding flow rates are 0.005, 0.01 and 0.015, respectively, which correspond to creeping flow. The variation of the coalescence efficiency with the residence time is shown in Fig. 6c, where the efficiency increases with the residence time, as expected. As E=200 V mm^{-1} is lower than the optimum field intensities of all the three waveforms, the coalescence is weak and the difference between different waveforms is not remarkable.   Obviously the residence time and flowrate used here cannot represent the industrial applications, for which further work is needed.

4. Model description

The efforts in the numerical analysis are directed towards the development of a rapid tool for assessing the effect of varying geometric and operational parameters of the V-shape electrodes on the coalescence process. The proprietary software Comsol Multiphysics is used to conduct the simulation. 2D simulations are first carried out on a simplified system corresponding to one stage of electrocoalescence between the electrodes. In the 2D domain, the droplets are considered as cylinders rather than spheres, which may have different dynamics from the 3D reality. Work reported in literature [35, 43-45] shows that 2D simulations can predict the droplet behaviour well. Nevertheless a comparison between 2D and 3D simulations is reported in the appendix to show the accuracy of the present study of droplet-droplet electrocoalescence. The electrodes are 10 mm apart and the applied voltage is 2 kV. The properties of sunflower oil are used for the continuous phase. The oil flow rate is 1.67 mm s^{-1}, i.e. the same as the experiment. The non-orthogonal 2D computational domain and the mesh are depicted in Figs. 7a and 7b, respectively. Fig. 7c shows the computational domain with inclination angles of 0°, 30°, 50° and 70°, respectively. Very fine meshes and 267326 grids are used, because accurate prediction of drop interface behavior needs fine meshes. The boundary conditions used in this paper are as follows: the upper electrode is subjected to the applied electric potential, while the lower one is kept earthed.　Both electrodes are set as wetted walls, as this allows the setting of the contact angle; the upper boundary has the velocity inlet, while the lower one has the pressure outlet; both the right and left boundaries have no-slip conditions. The Level-Set method is

employed to track the boundaries between continuous oil phase and dispersed water phase. The location of interface is obtained by solving the transport equation of the Level-Set function $\emptyset$. The interface is modelled as a diffuse boundary. A preliminary step computes the distance between the initial interface and the nodes of the computational domain, D_{si}. The initial condition for the time dependent study is then calculated as $\phi = \dfrac{1}{1+e^{\pm D_{si}/\xi}}$. The positive sign is used for points initially inside the interface, whereas the negative sign applies to the domain outside the interface. The interface is described by the Level-Set $\emptyset = 0.5$. The variable $\emptyset$ increases to 1 and decreases to 0 exponentially outside and inside the droplet, respectively. We follow the approach of Li et al. [20] and Vivacqua et al. [36], coupling Eq. (3) with the Navier Stokes equations for the flow and Laplace equations for the electric field.

$$\frac{\partial \phi}{\partial t} + \mathbf{u}\nabla\phi = \lambda\nabla\cdot(\xi\nabla\phi - \phi(1-\phi)\frac{\nabla\phi}{|\nabla\phi|}) \tag{3}$$

where $\mathbf{u}$ is fluid velocity, $\emptyset$ is a smooth step function which varies from 0 to 1, λ is the re-initialization parameter, which gives stability to the solution. Its value is set to 1 m/s in the present study. ξ (=$h_{max}/2$ in the present study, where h_{max} is the maximum mesh element size) is related to the interface thickness.

<Fig.7: (a) Sketch of the simulation domain. (b) Close-up of the mesh. (c) Sketch of the simulation domains with inclination angles of 0°, 30°, 50° and 70°, respectively.>

The capillary and electrostatic forces are also included in the Navier Stokes equations shown as follows.

$$\rho(\phi)\frac{\partial \mathbf{u}}{\partial t} + \rho(\phi)(\mathbf{u}\cdot\nabla)\mathbf{u} = -\nabla p + (\mu(\phi)(\nabla\mathbf{u}+\nabla\mathbf{u}^{\mathrm{T}})) + \mathbf{F}_{\gamma} + \mathbf{F}_{\mathbf{E}} \tag{4}$$

$$\nabla\cdot\mathbf{u} = 0 \tag{5}$$

$$\rho(\phi) = \rho_{\mathrm{w}} + (\rho_{\mathrm{o}} - \rho_{\mathrm{w}})\phi \tag{6}$$

$$\mu(\phi) = \mu_{\mathrm{w}} + (\mu_{\mathrm{o}} - \mu_{\mathrm{w}})\phi \tag{7}$$

where p is the fluid pressure, $\mathbf{F}_{\gamma}$ is the interfacial force of oil and water phase, $\mathbf{F_E}$ is the electric force, ρ_{w} is water phase density, ρ_{o} is oil phase density, μ_{w} is water phase viscosity and μ_{o} is oil phase viscosity.

The interfacial force ($\mathbf{F}_{\gamma}$) is calculated as derived by:

$$\mathbf{F}_{\gamma} = \nabla\cdot(\gamma(\mathbf{I}-(\mathbf{n}\mathbf{n}^{\mathrm{T}}))\delta) \tag{8}$$

where γ is the surface tension coefficient, $\mathbf{I}$ is the identity matrix, $\mathbf{n}$ is the interface normal, and δ is a smooth approximation of the Dirac function. $\mathbf{n}$ and δ are obtained by calculating Eq. (8) and (9), respectively:

$$\mathbf{n} = \frac{\nabla\phi}{|\nabla\phi|} \tag{9}$$

$$\delta = 6|\nabla\phi||\phi(1-\phi)| \tag{10}$$

The electric force is obtained from the divergence of the Maxwell stress tensor:

$$\mathbf{F}_{\mathbf{E}} = \nabla\cdot(\varepsilon(\phi)\mathbf{E}\mathbf{E}^{\mathrm{T}} - \frac{1}{2}\varepsilon(\phi)(\mathbf{E}\cdot\mathbf{E})\mathbf{I}) \tag{11}$$

$$\varepsilon(\phi) = \varepsilon_{\mathrm{w}} + (\varepsilon_{\mathrm{o}} - \varepsilon_{\mathrm{w}})\phi \tag{12}$$

where $\mathbf{E}$ is the electric field intensity, ε_{w} is water phase permittivity, ε_{o} is oil phase permittivity. In electrohydrodynamics, the electric filed intensity is irrotational ($\nabla\times\mathbf{E} = 0$). The Gauss law can be written in terms of the electric displacement ($\mathbf{D}=\varepsilon(\varphi)\mathbf{E}$) as:

$$\nabla\cdot\mathbf{D} = \nabla\cdot(\varepsilon(\emptyset)\mathbf{E}) = q^{v} \tag{13}$$

where q^{v} is the volume charge density. The charge density is advected with the fluid

flow and conducted according to the fluid conductivity using the following charge transportation equation:

$$\frac{\partial q^v}{\partial t} + \nabla \cdot (q^v \mathbf{u}) = \nabla \cdot (\sigma(\emptyset) \nabla \Psi) \tag{14}$$

$$\sigma(\emptyset) = \sigma_w + (\sigma_o - \sigma_w)\emptyset \tag{15}$$

where Ψ is the electric potential, σ_w is water phase conductivity, σ_o is oil phase conductivity.

5. Discussion

The coalescence performance obtained by pulsatile fields is better than that obtained by the constant field using the V-shaped electrode, when the electric field intensity and frequency are tuned to their optimal values. Vivacqua et al. [14] suggested that the oscillating deformation of droplets weakens the membrane between neighbouring droplets promoting its rupture. In addition, continued exposure to electric field is not required for two coalescing droplets after the interfacial film has been ruptured. Therefore, modulating the field frequency is an important method to optimise the separation efficiency with all waveforms. A number of works reported in literature [46-48] have provided models to explain the existence of the optimal frequency. It is remarkable that the optimal frequency of 100 Hz obtained in the current case (see Fig. 5) is consistent with the extent of deformation reported by Li et al.'s work [20]. Furthermore, Li et al. reported that at high frequencies, the oscillation amplitude of droplets is negligible. This is also in good qualitative agreement with Fig. 5, which shows decreasing coalescence efficiency at high frequencies. Interestingly, it can also

be seen from this figure that the frequency range 60-200 Hz, where the pulsatile electric fields perform better than the constant fields, is the same as that where a non-linear relationship of the deformation ratio versus the ratio of Weber Number and Ohnesorge Number is observed [20]. Another noteworthy point is that the sawtooth waveform has proved to perform best at the high conductivity of 3 g L^{-1} and low residence times (2 and 3s) among the pulsatile fields. The reason can be that having a lower RMS value (Table 1b), the probability of occurrence of droplet disintegration and short-circuiting is lower.

The coalescence behaviour of a population of droplets is simulated and the results are shown in Fig. 8a. 80 droplets with 0.8 mm droplet diameter are simulated. Larger droplets than those of the experiments (0.16 mm is the arithmetic mean diameter) are used here to make the computation faster. According to the calculation, as a result of electro-coalescence, very large drops are present after 3 s. They form mainly on the lower electrode, where they are on the verge of cascading down the electrode, a phenomenon which has also been observed experimentally. The largest three drops in Fig. 8a are the result of the coalescence of 9, 8 and 7 droplets, respectively. Assuming that these three drops can easily be separated downstream, the efficiency of the coalescence process on a number basis would be (9+8+7)/80×100=30%, which is in good agreement with what is measured experimentally (27 %). It can be seen from Fig. 8a that about 50% of the original 0.8 mm droplets undergo coalescence. Most of these coalescence events take place while the fluid is accelerating toward the central portion of the coalescer, which is a region of preferential flow. Consequently, the transit

time of droplets in the V-shaped electrodes is longer than the flat electrodes, in which the droplets go out of the electrodes straightaway. Most of the non-coalesced droplets that were initially placed at the bottom of the simulation domain exit without significant exposure to the electric field.

In Fig. 8b, coalescence is described in terms of a number of pairwise coalescence, defined as the number of coalescence events between droplets of equal size:

$$n_{\text{pair}} = \frac{\ln((d/d_{\text{ini}})^3)}{\ln 2} \tag{16}$$

where d_{ini} is the initial droplet size (0.8 mm). This analysis shows that most of the droplets which undergo coalescence are the result of one to two pairwise coalescence. This low value is due to the short simulation time (3 s), which is lower than the mean residence time between the electrodes (roughly $10/1.67 = 6$s).   The latter itself is very short, suggesting the necessity of the use of multiple electrodes arranged in a nested stack. In any case, this analysis has proved capable of reproducing, at least qualitatively, some findings that are observed during the experiments and can be used for rapid assessment of the design alternatives.

< Fig. 8: (a) Image sequence of droplet size evolution when a large number of droplets are simulated. The calculation conditions are: constant DC wave, E=200 V mm^{-1}, D=0.8 mm, and fluids properties are given in Table 1a. (b) Coalesced droplet population in terms of pairwise coalescence.>

The influence of inclination angle, electrode surface wettability, and central aperture of the V-shaped electrodes is addressed here based on the simulation results. A simplified system comprising one stage of electrocoalescence between two electrodes is analysed to save computational time. 15 droplets are initially placed between the electrodes. The performance of the V-shaped electrodes (inclination angle of 50°) and the flat ones (inclination angle of 0°) is compared in Fig. 9a. Two coalescence events take place with the flat electrodes, while six events take place with the V-shaped ones, which demonstrates the advantage of the V-shaped ones over the flat ones. Clearly, the inclination angle of the electrodes with respect to the axis is influential. In addition, inclination angles of 30° and 70° are simulated and the results are shown in Fig. 9b. The number of coalescence events increases first and then decreases with increasing inclination angle; the inclination angle of 50$^\mathrm{o}$ performs best in the present work.

The influence of the wettability of the electrodes is analysed considering two situations: contact angle $\theta_{\mathrm{water}}=\pi/4$ and $\theta_{\mathrm{oil}}=3\pi/4$; contact angle $\theta_{\mathrm{water}}=3\pi/4$ and $\theta_{\mathrm{oil}}=\pi/4$. Varying the values of the contact angles does not produce significant differences. The same number of coalescence events (6 events) take place, and most of them occur while the fluid is accelerated towards the central region of the coalescer, which is a region of preferential flow. Comparison of results in Fig. 9c reveals that, in the former case ($\theta_{\mathrm{water}}=\pi/4$ and $\theta_{\mathrm{oil}}=3\pi/4$), the droplets wet the electrode bar better and move slower, so that coalescence with the upcoming droplets takes place. In contrast, the same droplets in the latter case ($\theta_{\mathrm{water}}=3\pi/4$ and $\theta_{\mathrm{oil}}=\pi/4$) roll around the electrode bar and

the opportunity for coalescence is missed. For this reason, it seems that hydrophilic electrode surfaces would perform better.

<Fig. 9: (a) Image sequence of droplet size evolution with flat electrode and the V-shaped one ($\theta_{\text{water}}=\pi/4$ and $\theta_{\text{oil}}= 3\pi/4$). (b) Coalescence events at different inclination angles. (c) Different droplet behaviour with hydrophobic and hydrophilic electrode, respectively. The calculation conditions are: constant DC wave, E=200 V mm^{-1}, D=0.8 mm, and fluids properties are given in Table 1a.>

The outcomes of the simulation with a reduced central aperture which reduces the flow to the centre are shown in Fig. 10a. In this case only three coalescence events take place. These results illustrate that concentrating the water droplets in the central region can enhance their coalescence.

<Fig.10: (a) Image sequence of droplet size evolution with reduced central aperture. The calculation conditions are: constant DC wave, E=200 V mm^{-1}, D=0.8 mm, and fluids properties are given in Table 1a; (b) Snapshots at the outlet of the pilot plant coalescer: (i) no field applied; (ii) 50 V mm^{-1}. DC field. Flow rate: 20 L min^{-1}.>

Compared with the traditional electrodes widely used in commercial electrocoalescers [1, 11], there are specific advantages of the design tested here. The water-in-oil emulsion goes through the electrodes rather than flowing over them and the direction of the flow is roughly aligned with that of the external electric field. In contrast, with the emulsion flowing over and around the electrodes, the electric field is perpendicular to the flow direction, retarding the coalescence of pairwise droplets whose centre-line is parallel to the flow direction. In addition, the inclination of the V-shaped electrodes makes the water droplets rolling on the electrodes and directionally flowing to the central region of the coalescer, as observed by high speed video recording, thus enhancing phase separation. The structure of the electrodes can also hold up large droplets, at least temporarily, to form films. Therefore, both droplet-droplet and droplet-interface coalescence are promoted in this design. Both coalescence mechanisms due to dipole-dipole interaction and electrophoresis [14] are present. As this configuration allows nesting consecutive electrode elements [11] in a compact configuration, a significant reduction of the electrocoalescer volume can be obtained. The electrode design in the current work provides a two-dimensional set up. If extended to three-dimensional design, as proposed by Vivacqua et al [11], the electrodes can be made in the shape of conical frustum with metal wire mesh. Multiple electrodes can be nested together, forming a compact electrode set. The design of the electrodes can also allow the spacing between the electrodes to be varied easily. With the conical frustum electrodes [11], pilot-scale experiments with flow rate of 20 L min^{-1}, which is nearly three orders of magnitude larger than the one used in the lab-scale evaluation here (0.05

L min^{-1}), have been conducted at the University of Nottingham, UK. In Fig. 10b(i) practically no water drops are visible, but the oil contains some very fine droplets, due to a high level of emulsification while circulating in the by-pass loop of the water contaminated oil tank. Upon application of relatively small electric field (50 V mm^{-1}), some large drops start to appear at the outlet of the pilot plant coalescer (Fig. 10b(ii)). These results confirm the suitability of this technology when applied to the removal of trace water from crude oil. In addition, the results confirm the suitability of this design for using bare electrodes, as the electrode geometry can be configured such that the hydrodynamic conditions mitigate short-circuiting. The presence of bare electrodes ensures a higher rate of collision of droplets due to electrophoresis and dramatically increases the coalescence rate, by promoting dipole-dipole interaction, electrophoresis, and to a certain extent dielectrophoresis.   Insulating electrodes have a lesser effect and evaluation of their performance with V shape or conical frustum geometry design should be taken into consideration in future work.

6. Conclusions

In this work, the performance of a novel design of electrodes was assessed in terms of the coalescence efficiency. In this design, the emulsion goes through the electrodes rather than flowing over them. This enhances the electrical attractive force between neighbouring droplets and also provides a compact design with a short residence time. At the same time several sets of electrodes can be nested to improve the phase separation efficiency. Bare electrodes rather than insulated electrodes, which have been

widely utilized in recent designs, are used to improve the coalescence performance. The electrode bars can temporarily hold up large droplets to form water films on the electrode surface. Hence not only drop-drop coalescence but also drop-interface coalescence is promoted. The effect of electrical parameters (i.e. electric field intensity, frequency and waveform), fluid physical properties (i.e. conductivity and water content) and residence time on the coalescence efficiency were assessed. By tuning the electric field intensity and frequency, the coalescence efficiency under pulsatile fields can be significantly improved compared to constant DC fields using the V-shaped electrodes. With the current design, the hydrophilic electrodes perform better than the hydrophobic ones, and a reduced central aperture significantly impedes the extent of coalescence. The outcome of this work is potentially useful for optimizing the design of compact and efficient oil-water separators.

Appendix

The computational models use 2D and 3D domain, respectively, and schematically shown in Fig. 11a. The boundary conditions are as follows: the upper boundary is subjected to the applied electric potential, while the lower one is earthed and both boundaries have no-slip conditions; also both the the right and left boundaries have no-slip conditions. Very fine meshes, e.g. 28072 grids for the 2D simulations and 829720 grids for the 3D simulations, are used to predict the drop interface behaviour accurately. The experimental and numerical conditions are as follows: constant direct current (DC) wave, E=200 V mm^{-1} and D=0.8 mm. In the present study, the coalescence process of 2D and 3D simulations is compared with high speed video records of experimental work, as presented in Fig. 11b, where a good agreement is observed. Therefore, the 2D simulation carried out here can reproduce the 3D reality well and efficiently. However, the compatibility of the results of 2D and 3D calculations might be specific to the case at hand. It is therefore necessary to carry out a similar comparative exercise if the properties and conditions differ widely from those under consideration here.

< Fig. 11: (a) Sketch of the 2D and 3D simulation domains. (b) Pairwise droplet electrocoalescence obtained by experiment, 2D simulation and 3D simulation, respectively. The conditions for experimental work and numerical conditions are: constant DC wave, E=200 V mm^{-1}, D=0.8 mm, and fluids properties are given in Table 1a.>

References

[1] S. Mhatre, V. Vivacqua, M. Ghadiri, A.M. Abdullah, M.J. Al-Marri, A. Hassanpour, B. Hewakandamby, B. Azzopardi, B. Kermani, Electrostatic phase separation: a review. Chem. Eng. Res. Des. 96 (2015), 177-195.

[2] J.S. Eow, M. Ghadiri, Electrostatic enhancement of coalescence of water droplets in oil: a review of the technology. Chem. Eng. J. 85 (2-3) (2002), 357-368.

[3] B. Li, Y. Fan, Z. Sun, Z. Wang, L. Zhu, Effects of high-frequency pulsed electrical field and operating parameters on dehydration of SAGD produced ultra-heavy oil, Powder Technol. 316(2017)338-344.

[4] S.E. Taylor, Theory and practice of electrically-enhanced phase separation of water-in-oil emulsion, Trans. IChemE, 74 (5) (1996) 526-540.

[5] R.A. Mohammed, A.I. Baile, P.F. Luckham, S.E. Taylor, Dewatering of crude oil emulsions 3, Colloids Surf. A, 83 (3) (1994) 261-271.

[6] D. Sun, S.C. Jong, X.D. Duan, D. Zhou, Demulsification of water-in-oil emulsion by wetting coalescence materials in stirred-and-packed columns, Colloids Surf. A., 150 (1-3) (1999) 69-75.

[7] M. Goto, J. Irie, K. Kondo, F. Nakashio, Electrical demulsification of w/o emulsion by continuous tubular coalesce, J. Chem. Eng. Jpn., 22 (4) (1989) 401-406.

[8] T. Hirato, K. Koyama, T. Tanaka, Demulsification of water-in-oil emulsion by an electrostatic coalescence method, Mater Trans.32 (3) (1991) 257-263.

[9] K. Guo, Y. Lü, L. He, X. Luo, D. Yang, Separation characteristics of W/O emulsion under the coupling of electric field and magnetic field, Energy & Fuels, 33 (2019)

2565-2574.

[10] O. Urdahl, N.J. Wayth, H. Førdedal, T.J. Williams, A.G. Bailey, (2001), Compact electrostatic coalescer technology. In: Sjöblom,J. (Ed.), Encyclopedic Handbook of Emulsion Technology. Marcel Dekker, New York.

[11] V. Vivacqua, M. Ghadiri, A.M. Abdullah, A. Hassanpour, M.J. Al-Marri, B. Azzopardi, B. Hewakandamby, and B. Kermani, Compact electrocoalescer with conical frustum electrodes, (2016), US Provisional Application No. 62/425,808.

[12] P.J. Bailes, An experimental investigation into the use of high voltage DC fields for liquid phase separation, Trans. I Chem. E 59 (4) (1981) 229-237.

[13] P.J. Bailes, D. Freestone, G.W. Sams, Pulsed DC fields for electrostatic coalescence of water-in-oil emulsions, Chem. Eng. 644 (1997) 34-39.

[14] V. Vivacqua, S. Mhatre, M. Ghadiri, A.M. Abdullah, A. Hassanpour, M.J. AI-Marri, B. Azzopardi, B. Hewakandamby, B. Kermani, Electrocoalescence of water drop trains in oil under constant and pulsatile electric fields, Chem. Eng. Res. Des. 104 (2015) 658-668.

[15] S.H. Mousavi, M. Ghadiri, M. Buckley, Electro-coalescence of water drops in oils under pulsatile electric fields, Chem. Eng. Sci. 120 (2014) 130-142.

[16] L. Lundgaard, G. Berg, A. Pedersen, P.J. Nielsen, (2002) Electrocoalescence of water drop pairs in oil. In: Proceedings of the 14th International Conference on Dielectric Liquids, Graz, Austria.

[17] C. Lesaint, W.R. Glomm, L.E. Lundgaard, J. Sjöblom, Dehydration efficiency of AC electrical fields on water-in-model-oil emulsions. Colloids Surf. A:

Physicochem. Eng. Aspects 352 (2009) 63-69.

[18] G. Berg, L.E. Lundgaard, M. Becidan, R.S. Sigmond, (2002) Instability of electrically stressed water droplets in oil. In: Proceedings of the 14th International Conference on Dielectric Liquids, Graz, Austria.

[19] S. Ingebrigtsen, G. Berg, L.E. Lundgaard, (2005) Electrocoalescence in stagnant emulsions dielectric liquids. In: IEEE International Conference.

[20] B. Li, V. Vivacqua, M. Ghadiri, Z. Sun, Z. Wang, X. Li, Droplet deformation under pulsatile electric fields, Chem. Eng. Res. Des. 127 (2017) 180-188.

[21] T.J. Williams, A.G. Bailey, Changes in the size distribution of a water-in-oil emulsion due to electric field induced coalescence. IEEE Trans. Ind. Appl. 1A-22 (3) (1986), 536-541.

[22] M. Mousavichoubeh, M. Ghadiri, M. Shariaty-Niassar, Electro-coalescence of an aqueous droplet at an oil-water interface, Chem. Eng. Process. 50 (3) (2011) 338-344.

[23] M. Mousavichoubeh, M. Shariaty-Niassar, M. Ghadiri, The effect of interfacial tension on secondary drop formation in electro-coalescence of water droplets in oil, Chem. Eng. Sci. 66 (21) (2011) 5330-5337.

[24] X. Luo, H. Xin, H. Yan, D. Yang, W. Jing, L. He, Breakup Modes and Criterion of Droplet with Surfactant under Direct Current Electric Field, Chem. Eng. Res. Des. 132 (2018) 822-830.

[25] D. Wang, J. Wang, X. Wang, Y. Huo, P. Yongphet, Experimental investigation on the deformation and breakup of charged droplets in dielectric liquid medium,

International Journal of Multiphase Flow, 114 (2019) 39-49.

[26] J.A. Lanauze, R. Sengupta, B.J. Bleier, B.A. Yezer, L. Walker, Colloidal stability dictates drop breakup under electric fields, Soft Matter, 14 (2018) 9351-9360.

[27] Y. Huo, J. Wang, H. Qiu, Z. Zuo, Y. Fan, Noncontact rebound and fission of oppositely charged droplets, Experiments in Fluids, 56 (2015) 65.

[28] Y. Huo, J. Wang, W. Mao, Z. Wang, Z. Zuo, Measurement and investigation on the deformation and air-assisted breakup of charged droplet, Flow Measurement and Instrumentation, 27 (2012) 92-98.

[29] A.H. Brown, C. Hanson, Effect of oscillating electric fields on coalescence in liquid-liquid systems. Trans. Faraday Soc.61 (1965) 1754-1760.

[30] X. Luo, H. Yin, H. Yan, X. Huang, D. Yang, L. He, The electrocoalescence behavior of surfactant-laden droplet pairs in oil under a DC electric field, Chem. Eng. Sci. 191 (2018) 350-357.

[31] S. Mhatre, S. Simon, J. Sjöblom, Shape evolution of a water drop in asphaltene solution under weak DC electric fields, Chem. Eng. Res. Des. 141 (2019) 540-549.

[32] Z. Wang, K. Dong, L. Tian, J. Wang, J. Tu, Numerical study on coalescence behavior of suspended drop pair in viscous liquid under uniform electric field, AIP Advances, 8 (2018) 085215.

[33] Z. Wang, Q. Dong, Y. Zhang, J. Wang, J. Wen, Numerical Study on Deformation and Interior Flow of a Droplet Suspended in Viscous Liquid under Steady Electric Fields, Advances in Mechanical Engineering, 2014 (2014) 1-12.

[34] Z. Wang, T. Guo, L. Tian, Q. Xu, S. Zhan, J. Tu, Numerical simulation on

circulation flow and mass transfer inside atmospheric water drops, Applied Thermal Engineering, 118 (2017) 765-772.

[35] L. He, X. Huang, X. Luo, H. Yan, Y. Lu, D. Yang, Y. Han, Numerical study on transient response of droplet deformation in a steady electric field, J. Electrost. 82 (2016) 29-37.

[36] V. Vivacqua, M. Ghadiri, A.M. Abdullah, A. Hassanpour, M.J. AI-Marri, B. Azzopardi, B. Hewakandamby, B. Kermani, Analysis of partial electrocoalescence by Level-Set and finite element methods, Chem. Eng. Res. Des. 114(2016) 180-189.

[37] B.S. Hamlin, J.C. Creasey, W.D. Ristenpart, Electrically tunable partial coalescence of oppositely charged drops. Phys. Rev. Lett. 109 (9) (2012) 094501.

[38] Y. Zhang, Y. Liu, R. Ji, B. Cai, H. Li, F. Wang, Dehydration efficiency of water-in-model oil emulsions in high frequency pulsed DC electrical field: effect of physical and chemical properties of the emulsions, J. Disper. Sci. Technol. 33 (2012) 1574-1581.

[39] J.S. Eow, M. Ghadiri, Drop/drop coalescence in an electric field: the effects of applied electric field and electrode geometry, Colloids and Surfaces A: Physicochem. Eng. Aspects, 219 (2003) 253-279.

[40] J. Xu, B. Li, Z. Sun, Z. Wang, B. Liu, M. Zhang, Effects of electrode geometry on emulsion dehydration efficiency, Colloids and Surfaces A: Physicochem. Eng. Aspects, 567 (2019) 260-270.

[41] Z. Wang, X. Lei, S. Zhan, Experimental Study on Electrohydrodynamics (EHD)

Spraying of Ethanol with Double-capillary, Applied Thermal Engineering, 120 (2017) 474-483.

[42] I.G. Harpur, N.J. Wayth, A.G. Bailey, M.T. Thew, T.J. Williams, O. Urdahl, Destabilisation of water-in-oil emulsions under the influence of an A.C. electric field: Experimental assessment of performance, J. Electrost. 40-41 (1997) 135-140.

[43] Q. Dong, A. Sau, Electrohydrodynamic interaction, deformation, and coalescence of suspended drop pairs at varied angle of incidence, 3 (2018) 073701.

[44] Q. Dong, A. Sau, Breakup of a leaky dielectric drop in a uniform electric field, 99 (2019) 043106.

[45] M. Chiesa, J. Melheim, A. Pedersen, S. Ingebrigtsen, G. Berg, Forces acting on water droplets falling in oil under the influence of an electric field: numerical predictions versus experimental observations, 24 (2005) 717-732.

[46] F.M. Joos, R.W. Snaddon, On the frequency dependence of electrically enhanced emulsion separation. Chem. Eng. Res. Des. 63 (5) (1985), 305-311.

[47] P.J. Bailes, An electrical model for coalescers that employ pulsed dc fields, Trans. IChemE 73 (A) (1995), 559-566.

[48] O-M. Midtgard, Electrostatic field theory and circuitanalysis in the design of coalescers with pulsed dc voltage. Chem. Eng. J. 151 (2009), 168-175.

(a)

(b)
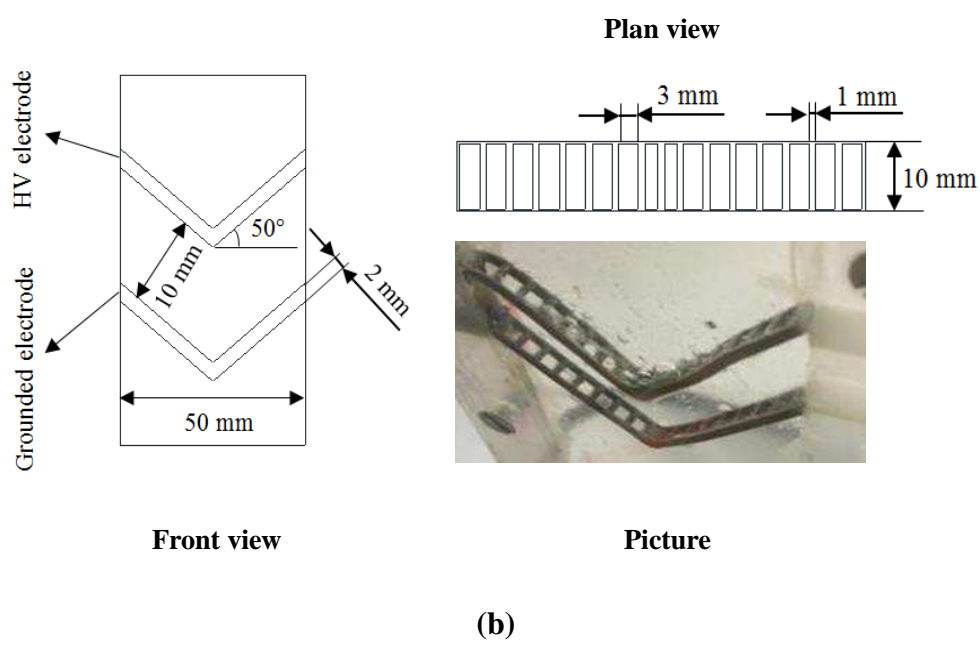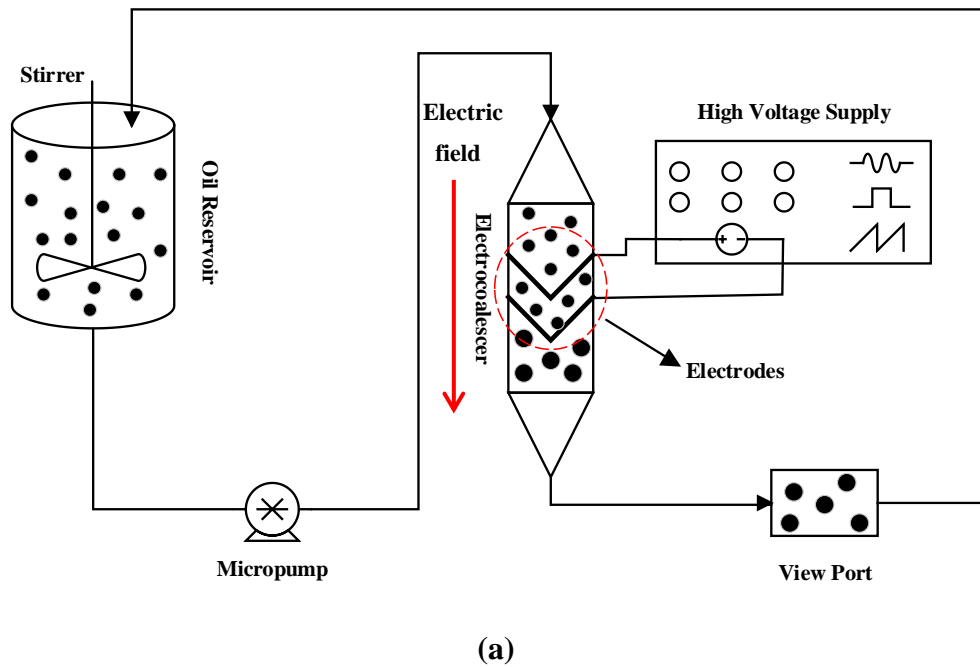
Fig.1 Experimental rig and electrode design
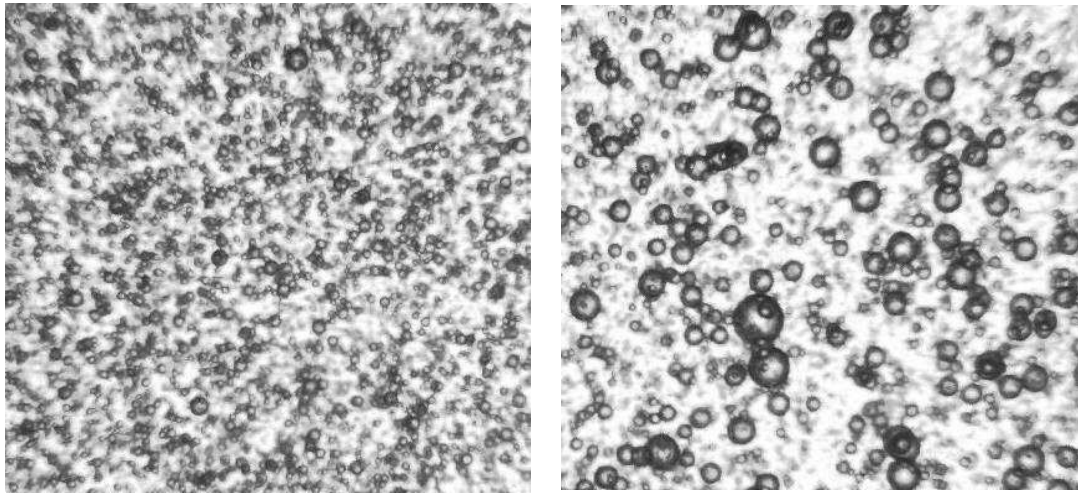
(a)   (b)
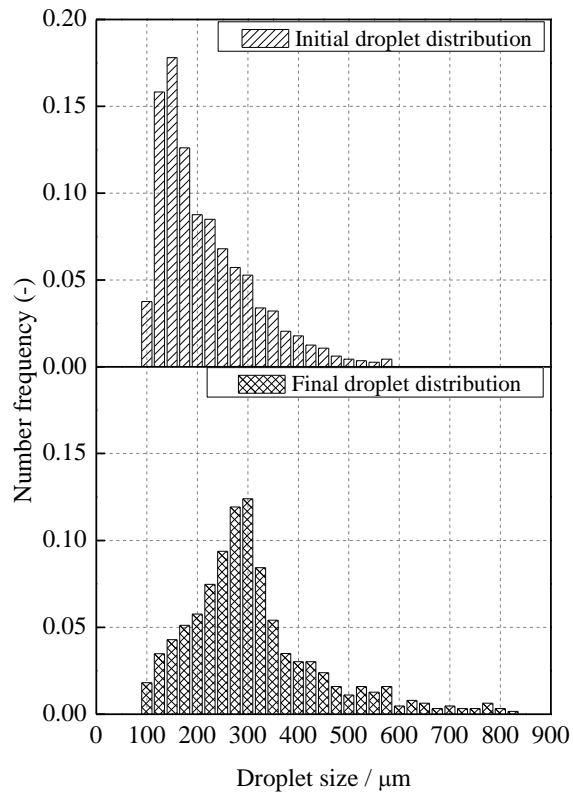
(c)

Fig.2 Representative snapshots of emulsion from the view port and initial droplet size distribution. (a): in the absence of electric field; (b): after the application of the electric field; (c): droplet size distribution (by number) before and after the application of electric field. The experimental conditions are: sunflower oil with 2 vol% deionised water; constant waveform; electric field intensity (E) of 200 V mm⁻¹.
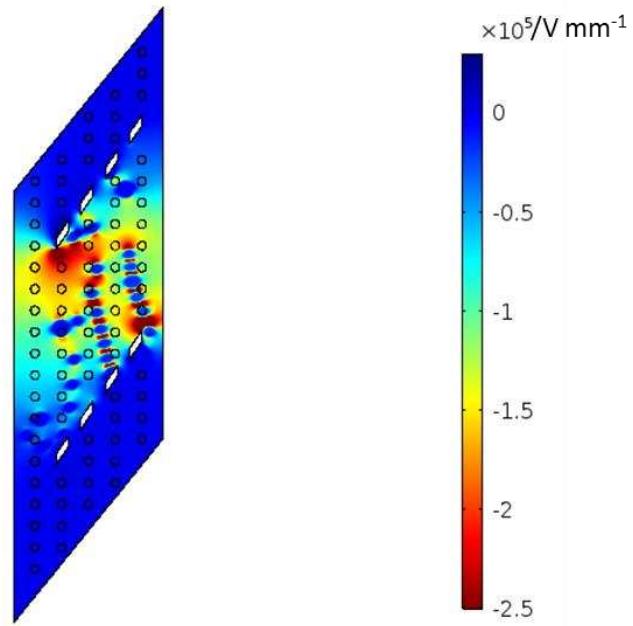
(a)
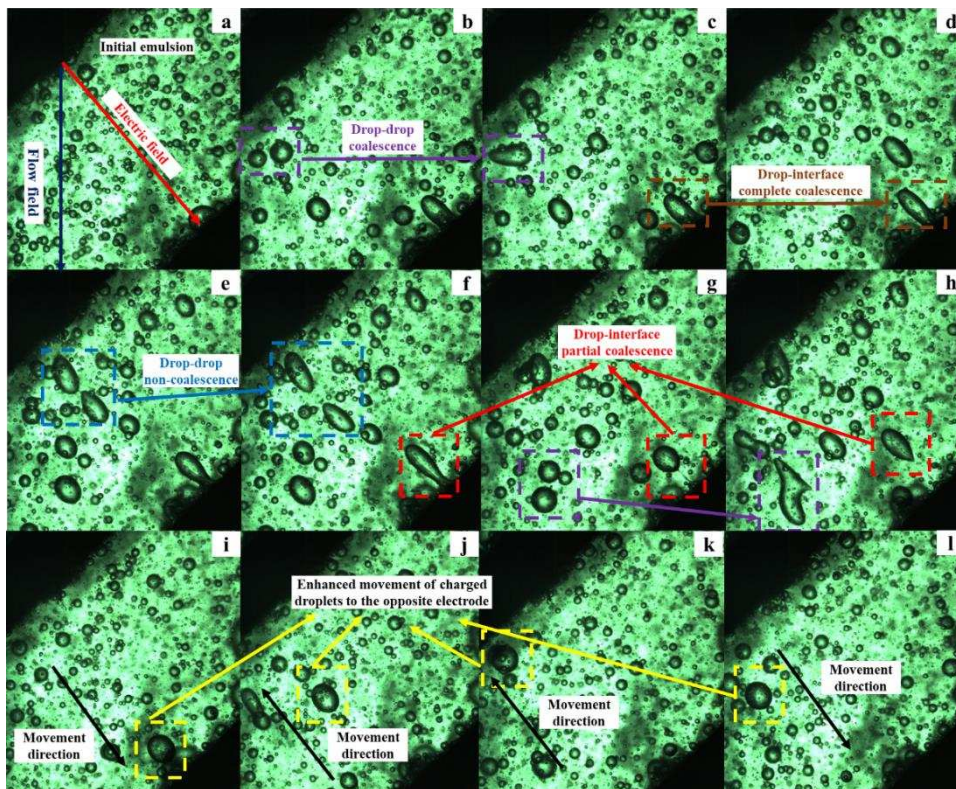
(b)

Fig. 3: (a) Electric field distribution at the average electric field intensity (E) of 200 V mm⁻¹ at t=1.5 s. (b)Snapshots of droplet behaviour between the V-Shape electrodes. The experimental conditions are: square waveforms; f=10 Hz; E=200 V mm⁻¹.
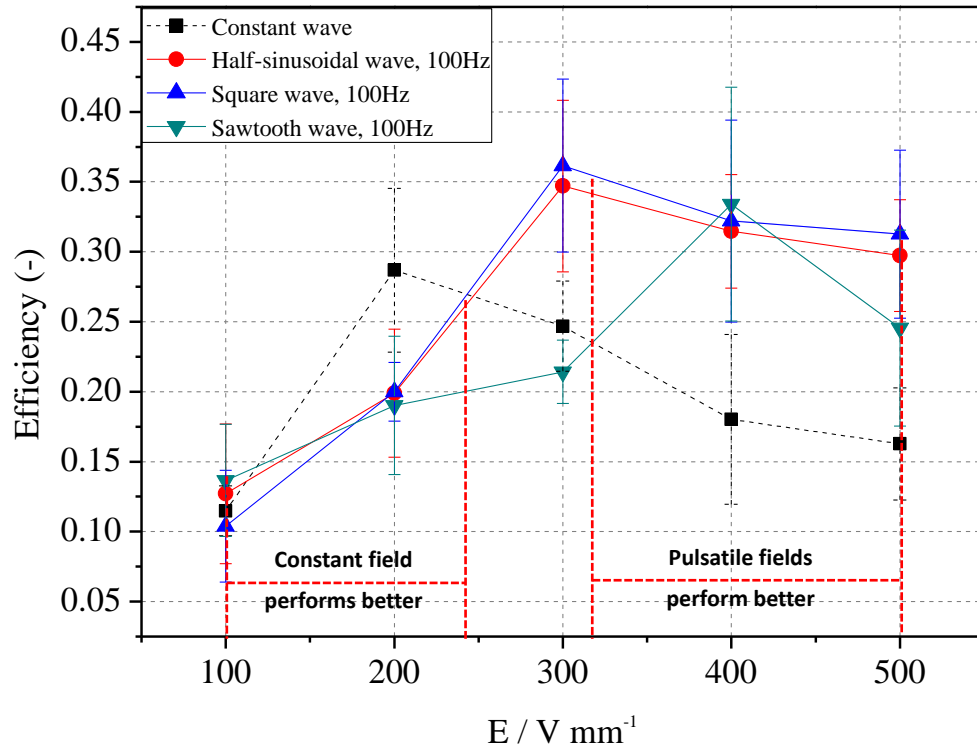
(a)
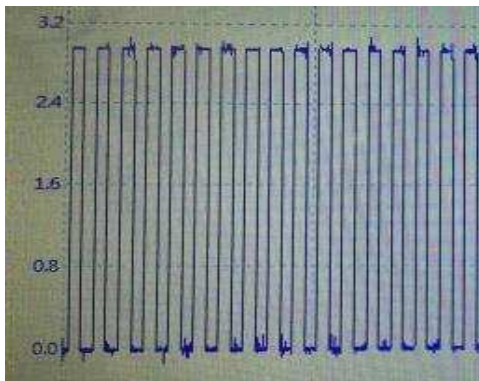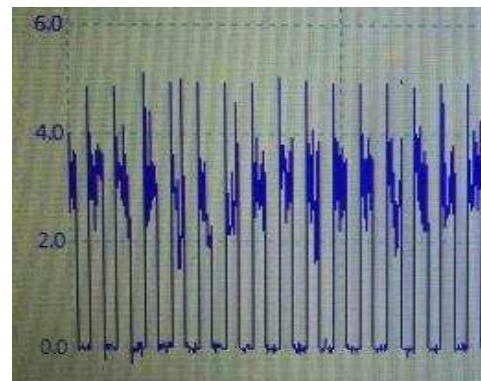
(i)　　　　　　　　　　　　　　　　　　　**(ii)**

(b)

Fig. 4: (a) Coalescence efficiency with half-sinusoidal, square and sawtooth DC fields at varying electric field intensity. The electric field frequency applied is the optimum frequency of 100 Hz for all the three pulsatile waveforms. Comparison with constant DC fields. (c) Snapshots of experimental electric intensities applied to the emulsions: (i) Square waveform, 5 Hz, 300 V mm^{-1}; (ii) Square waveform, 5 Hz, 500 V mm^{-1}.
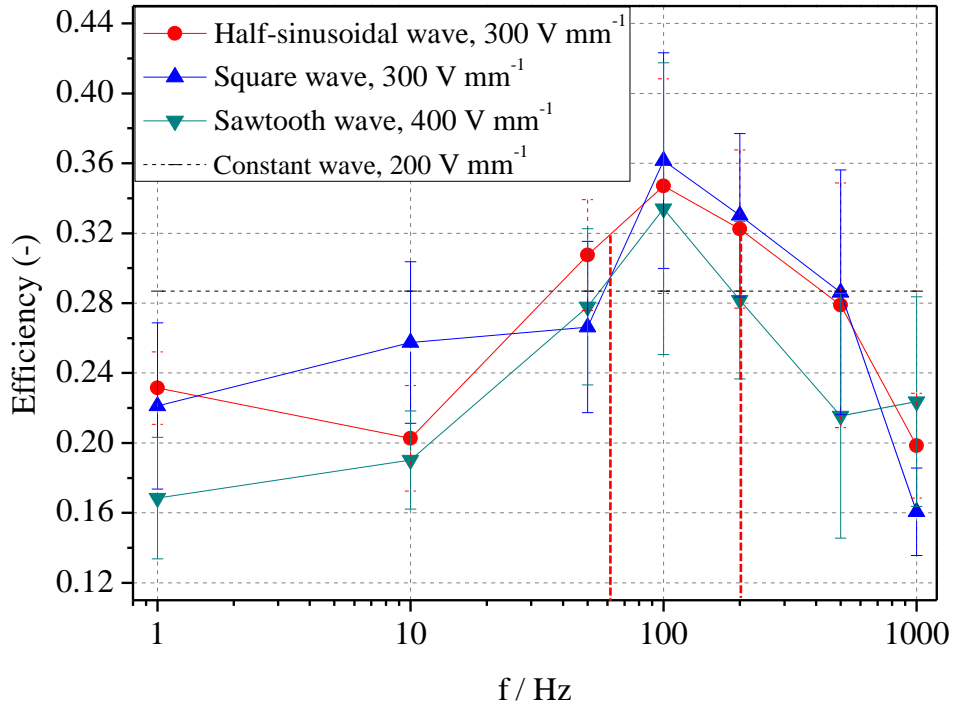
Fig. 5 Coalescence efficiency with half-sinusoidal, square and sawtooth DC fields at varying electric field frequency. The applied electric field intensities are the optimum values: half-sinusoidal and square wave of 300 V mm⁻¹, sawtooth wave of 400 V mm⁻¹. Comparison with constant DC fields of 200 V mm⁻¹.

Fig. 6: (a) Coalescence efficiency with half-sinusoidal, square and sawtooth DC fields at varying NaCl concentration. (b) Coalescence efficiency with half-sinusoidal, square and sawtooth DC fields at varying water concentration. (c) Coalescence efficiency with half-sinusoidal, square and sawtooth DC fields at varying residence time. The electric field intensities and frequencies applied are 200 V mm^{-1} and 100 Hz, respectively, for all the three waveforms.
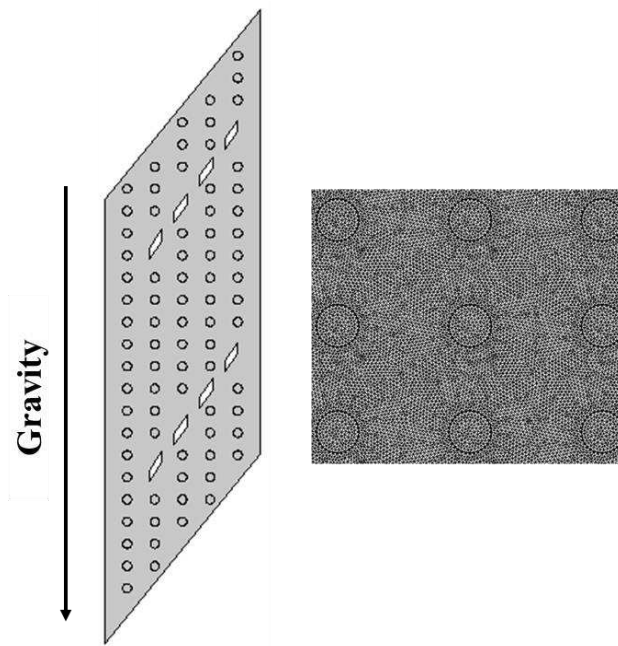
(a)   **(b)**
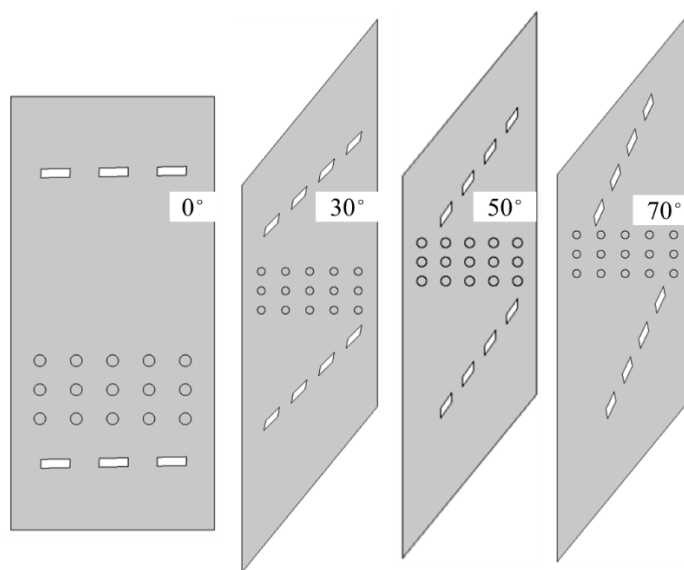
(c)

Fig.7: (a) Sketch of the simulation domain (inclination angle of 50 degree). (b) Close-up of the mesh. (c) Sketch of the simulation domains with inclination angles of 0°, 30°, 50° and 70°, respectively.
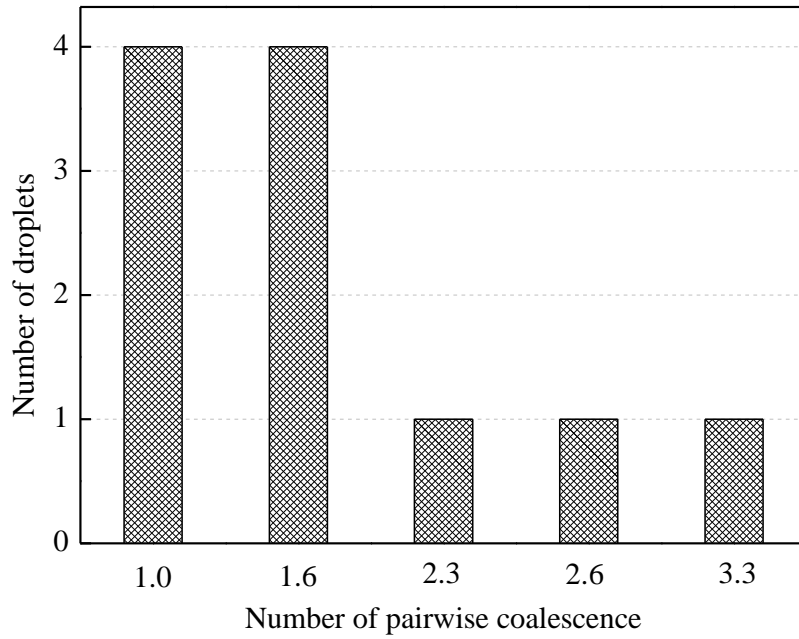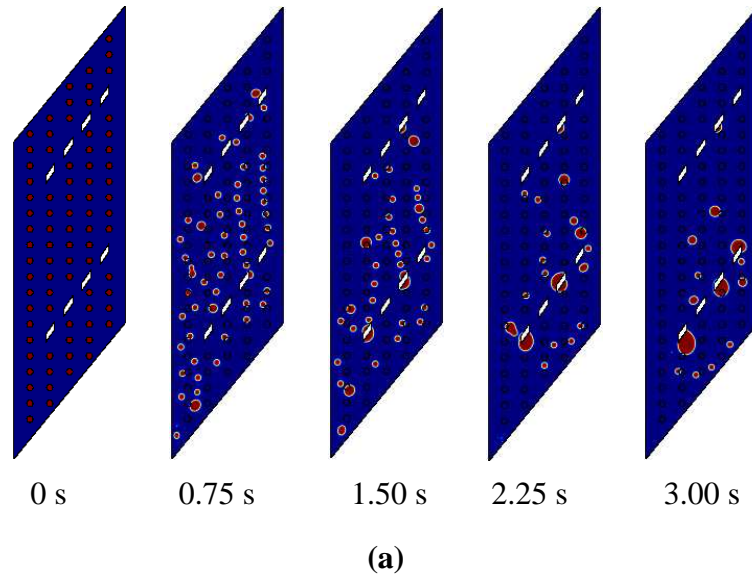
0 s   0.75 s   1.50 s   2.25 s   3.00 s

(a)

(b)

Fig. 8: (a) Image sequence of droplet size evolution when a large number of droplets are simulated. The calculation conditions are: constant DC wave, E=200 V mm⁻¹, D=0.8 mm, and fluids properties are given in Table 1. (b) Coalesced droplet population in terms of pairwise coalescence.
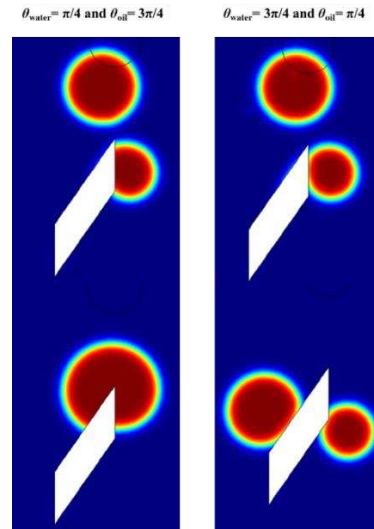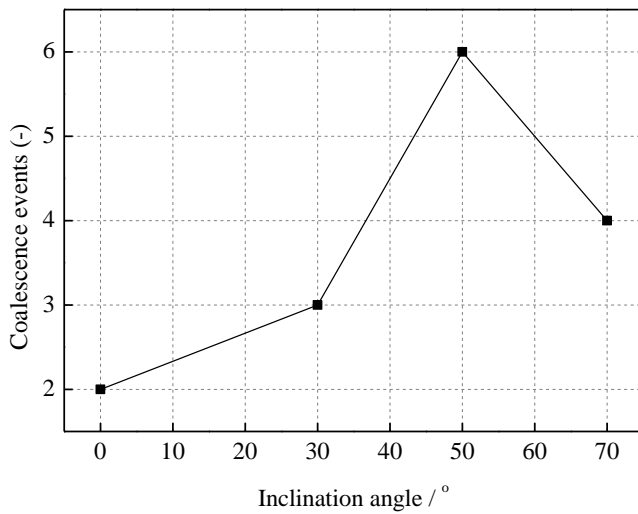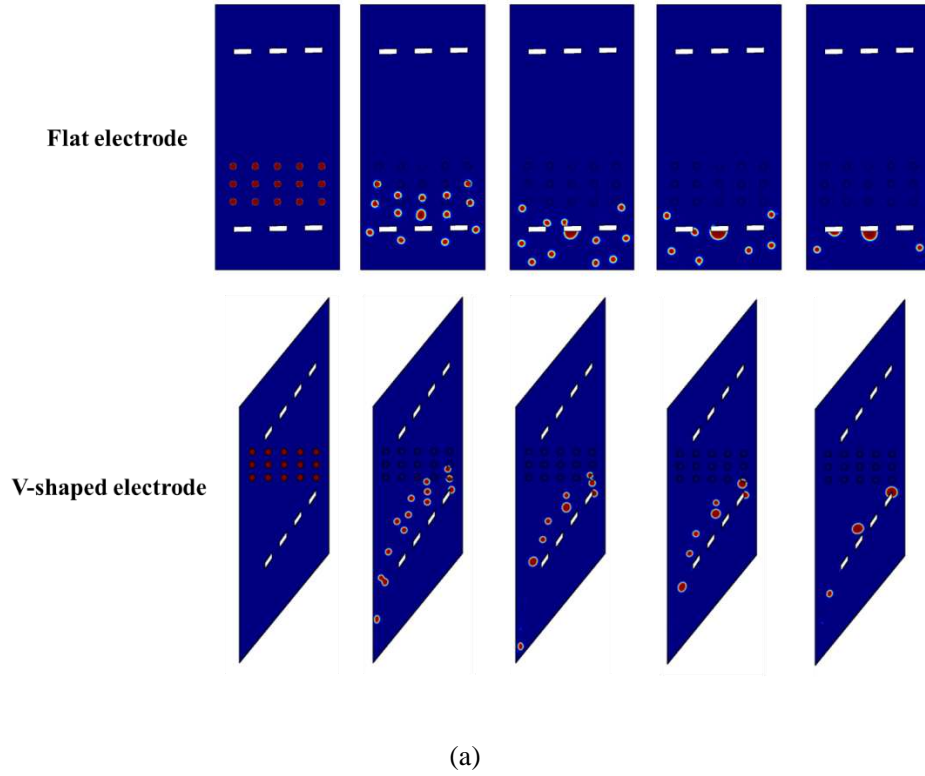
(a)

(b)

(c)

Fig. 9: (a) Image sequence of droplet size evolution with flat electrode and the V-shaped one (θ_{water}=π/4 and θ_{oil}= 3π/4). (b) Coalescence events at different inclination angles. (c) Different droplet behaviour with hydrophilic and hydrophobic electrode, respectively. The calculation conditions are: constant DC wave, E=200 V mm^{-1}, D=0.8 mm, and fluids properties are given in Table 1a.
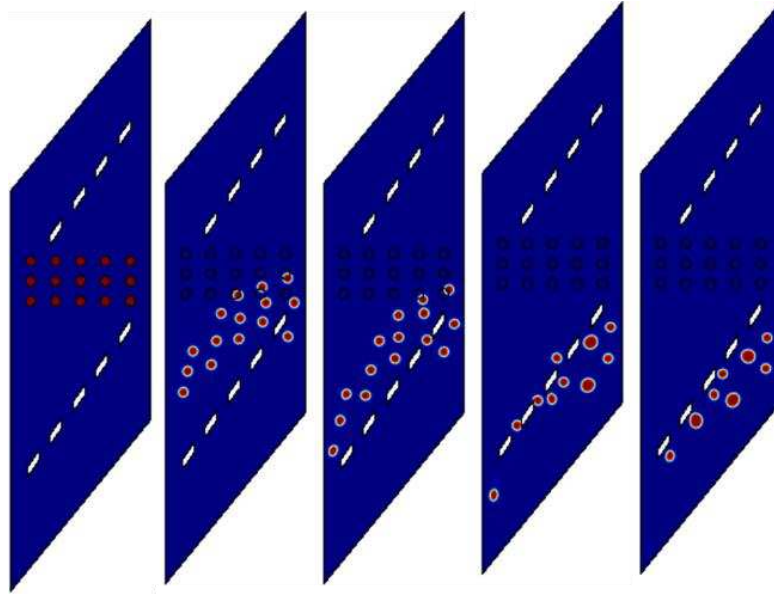
(a)
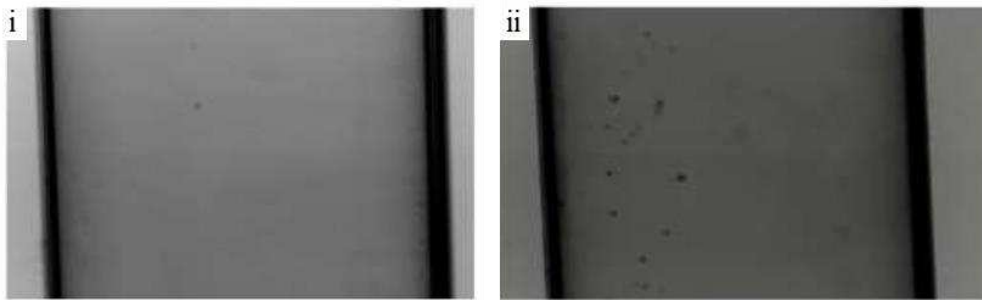
(b)

**Fig.10: (a) Image sequence of droplet size evolution with reduced central aperture. The calculation conditions are: constant DC wave, E=200 V mm⁻¹, D=0.8 mm, and fluids properties are given in Table 1a; (b) Snapshots at the outlet of the pilot plant coalescer: (i) no field applied; (ii) 50 V mm⁻¹. DC field. Flow rate: 20 L min⁻¹.**
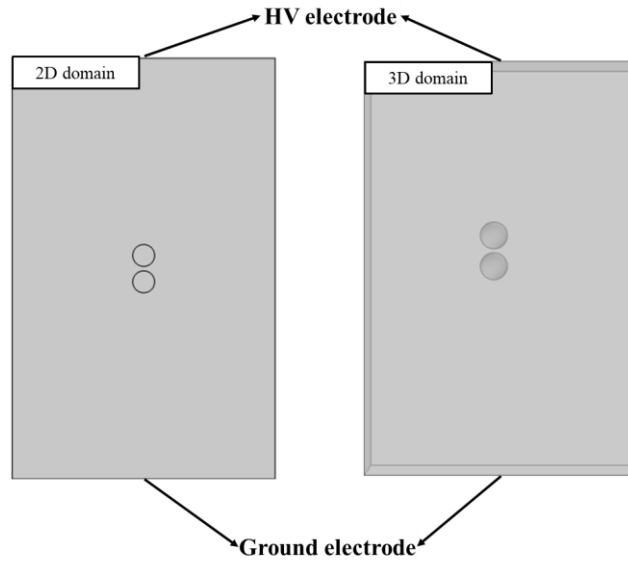
(a)
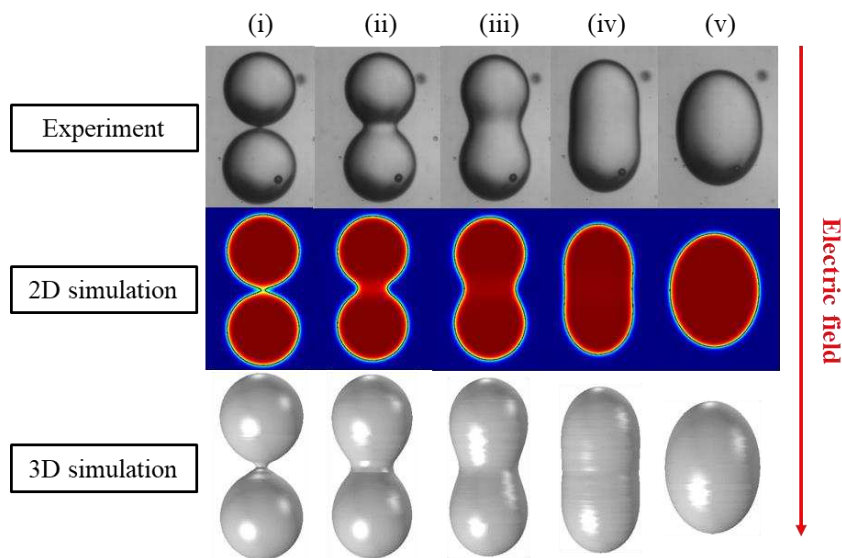
(b)

Fig. 11: (a) Sketch of the 2D and 3D simulation domains. (b) Pairwise droplet electrocoalescence obtained by experiment, 2D simulation and 3D simulation, respectively. The conditions for experimental work and numerical conditions are: constant DC wave, E=200 V mm^{-1}, D=0.8 mm, and fluids properties are given in Table 1a.

Liquid	Conductivity (μs m^{-1}) ($\pm 5\%$)	Viscosity (mPa s)	Density (kg m^{-3})	Dielectric constant
Deionised water	5.49	1.0	1000	80.0
Sunflower oil	7.62×10^{-5}	46.5	922	4.9

(a)

Waveform	RMS
Half-sinusodial	$E_0 (\sqrt{2}/2)$
Square	$E_0 (\sqrt{2}/2)$
Sawtooth	$E_0 (\sqrt{3}/3)$
Constant	E_0

(b)

NaCl concentration / g L^{-1}	0.00	1.00	2.00	3.00
Conductivity / μs m^{-1}	5.49	20.00	38.50	56.50

(c)

Table 1: (a) Physical properties of the emulsion; (b) Theoretical RMS values of the different electric field waveforms; (c) Deionised water conductivity with different NaCl concentrations